

Supplementary Materials for
**Anion exchange-induced single-molecule dispersion of cobalt
porphyrins in a cationic porous organic polymer for enhanced
electrochemical CO₂ reduction via secondary-coordination
sphere interactions**

Jia-Kang Tang^a, Chen-Yuan Zhu^a, Tian-Wen Jiang^a, Lei Wei^b Hui Wang^a,
Ke Yu^c, Chun-Lei Yang^a, Yue-Biao Zhang^b, Chen Chen^c,
Zhan-Ting Li^a, Dan-Wei Zhang^{a*} and Li-Ming Zhang^{a*}

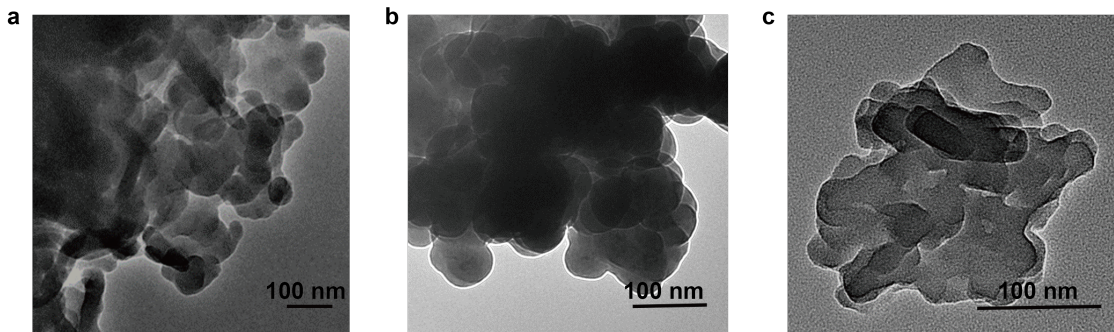


Figure S1 TEM images of POP-Py(0) (a), POP-Py(1) (b) and POP-Py(2) (c). The relatively small size of POP-Py(2) is possibly due to the low degree of polymerization caused by the low solubility of Di(4-pyridyl)biphenyl in NMP solution.

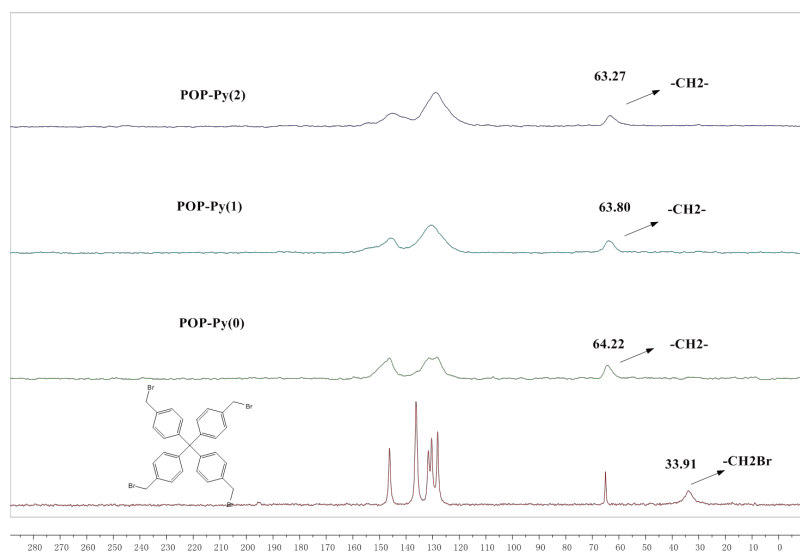


Figure S2 CP/MAS ^{13}C NMR spectrum of TBM, POP-Py(0), POP-Py(1) and POP-Py(2).

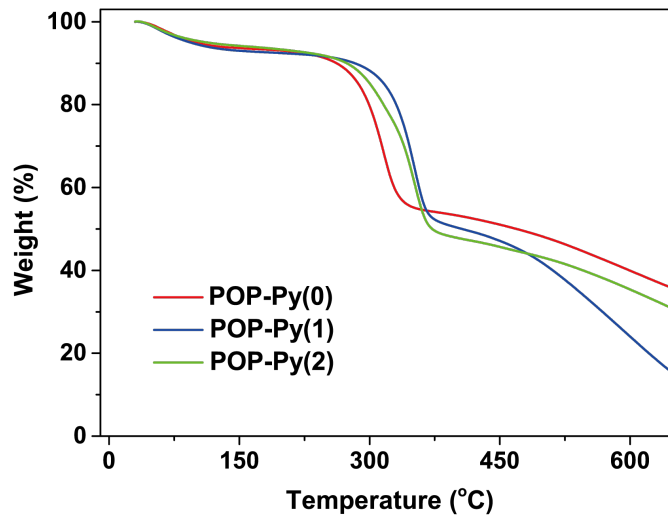


Figure S3 TGA profile of POP-Py(0) , POP-Py(1) and POP-Py(2) under N₂ atmosphere.

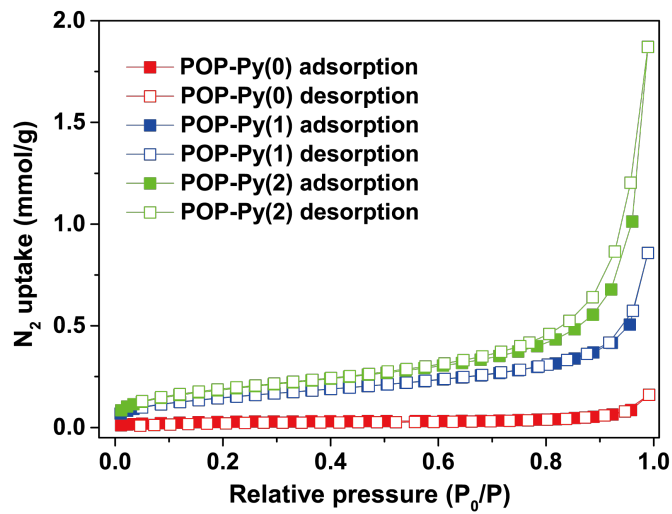


Figure S4 Nitrogen adsorption/desorption isotherms of POP-Py(0), POP-Py(1) and POP-Py(2) at 77 K.

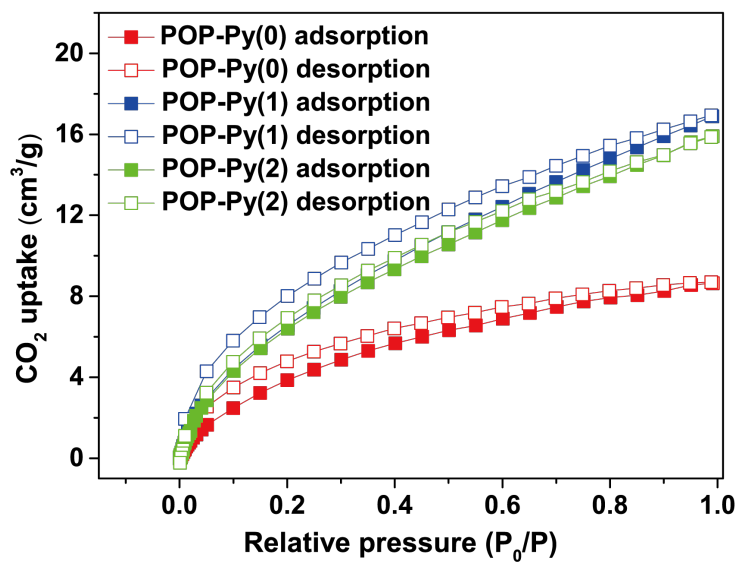


Figure S5 CO_2 adsorption/desorption isotherms of POP-Py(0), POP-Py(1) and POP-Py(2) at 298 K.

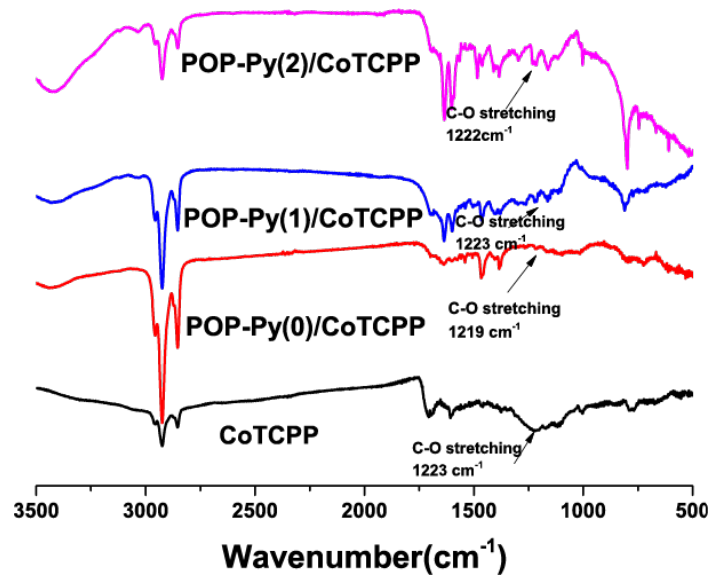


Figure S6 FT-IR spectra of CoTCPP, POP-Py(0)/CoTCPP, POP-Py(1)/CoTCPP and POP-Py(2)/CoTCPP.

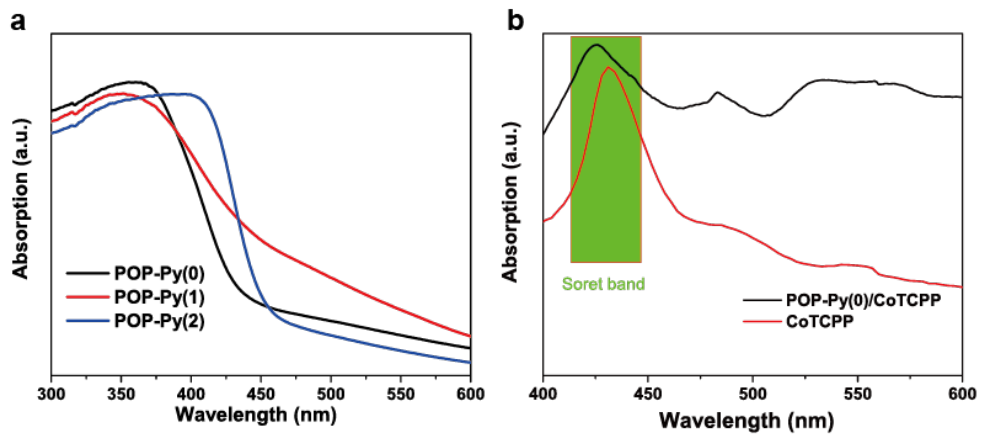


Figure S7 UV-vis spectra of (a) POP-Py(n); (b) CoTCPP and POP-Py(0)/CoTCPP.

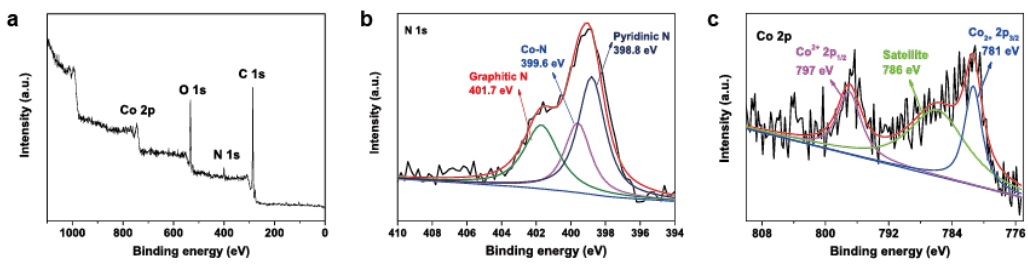


Figure S8 XPS survey (a), high-resolution N 1s (b) and Co 2p (c) spectra of POP-Py(0)/CoTCPP.

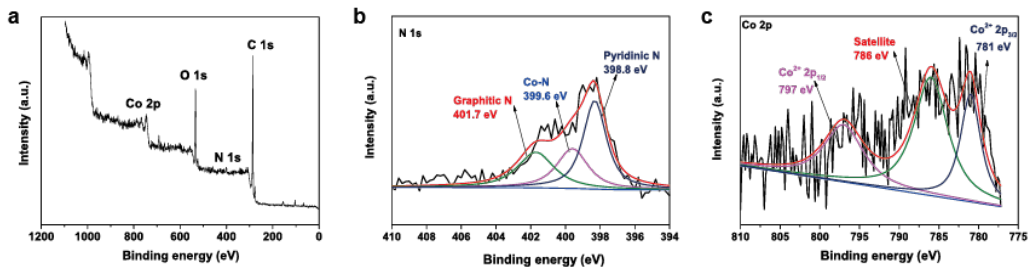


Figure S9 XPS survey (a), high-resolution N 1s (b) and Co 2p (c) spectra of POP-Py(1)/CoTCPP.

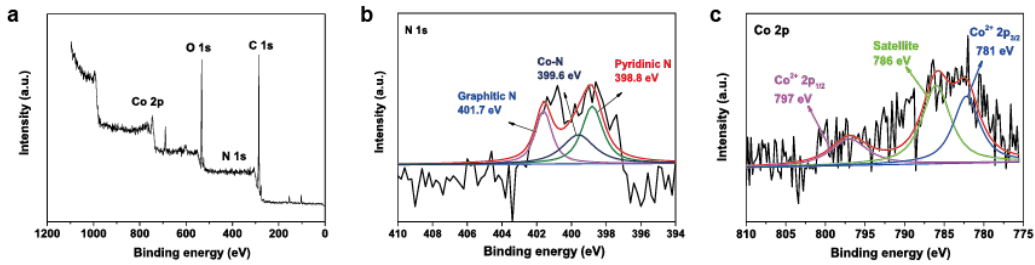


Figure S10 XPS survey (a), high-resolution N 1s (b) and Co 2p (c) spectra of POP-Py(2)/CoTCPP.

Table S1 Anion exchange efficiencies quantified by XPS

	POP-Py(0)/CoTCPP	POP-Py(1)/CoTCPP	POP-Py(2)/CoTCPP
Bromide/porphyrin ratio after exchange	0.39	0.58	0.40
Exchange efficiency	84%	78%	83%
$n_{\text{Br exchange}}/n_{\text{Br total}}$			

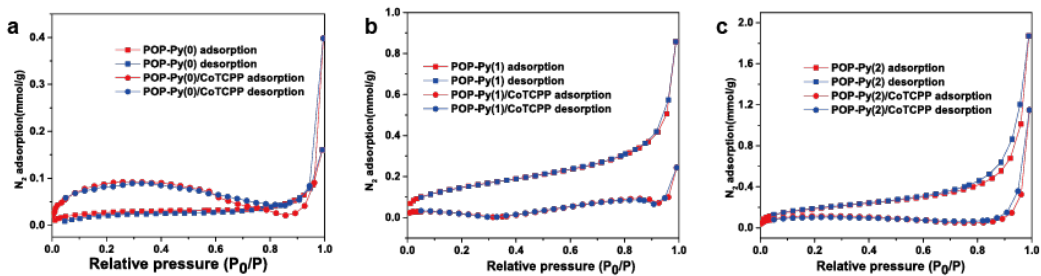


Figure S11 Nitrogen adsorption/desorption isotherms of (a) POP-Py(0) and POP-Py(0)/CoTCPP; (b) POP-Py(1) and POP-Py(1)/CoTCPP; (c) POP-Py(2) and POP-Py(2)/CoTCPP at 77 K.

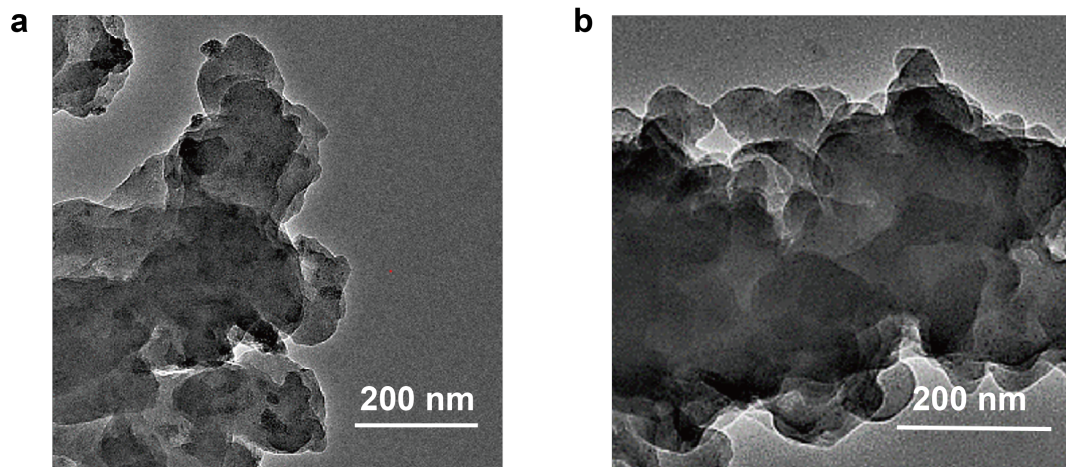


Figure S12 TEM images of POP-Py(1) (a) and POP-Py(2) (b).

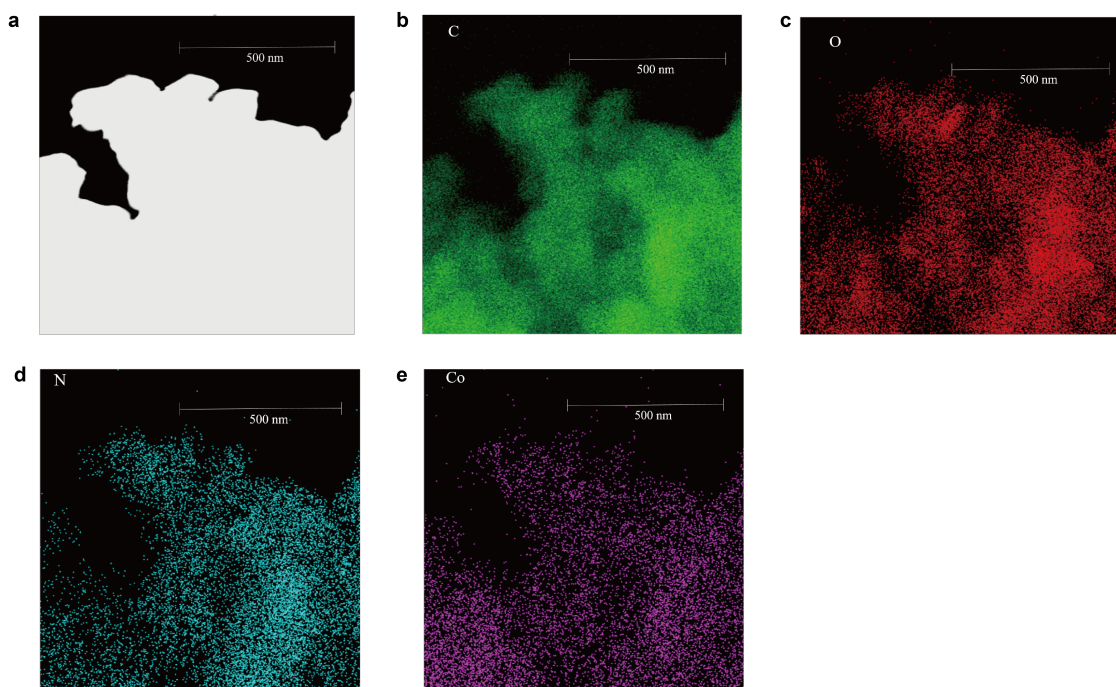


Figure S13 STEM image (a) of POP-Py(1)/CoTCPP and the EDX elemental mapping of C (b), O (c), N (d) and Co (e).

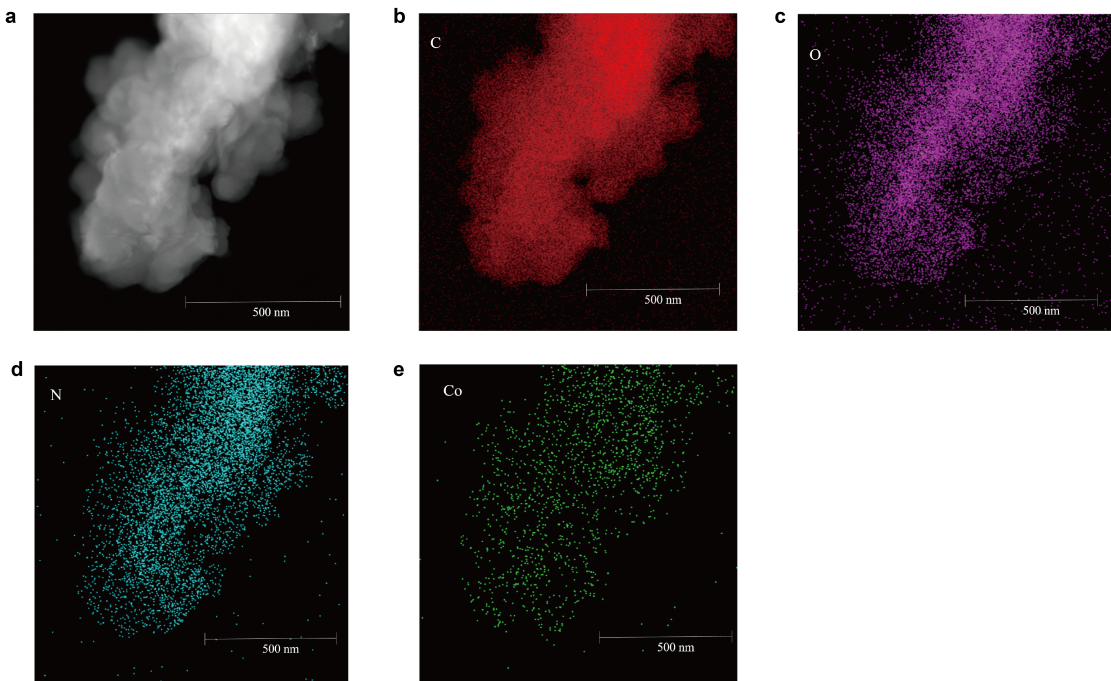


Figure S14 STEM image (a) of POP-Py(2)/CoTCPP and the EDX elemental mapping of C (b), O (c), N (d) and Co (e).

Table S2 Contents of CoTCPP in the hybrid catalysts determined by ICP-AES

Initial CoTCPP/carbon weight ratio before mixing	Mass percentage of Co in the hybrid (%)	Mass percentage of CoTCPP in the hybrid (%)	Catalyst loading drop-casted in the paper (mol/cm ²)
CoTCPP/POP-Py(0)=1/1	0.279	4.2	1.42*10 ⁻⁸
CoTCPP/POP-Py(1)=1/1	0.101	1.53	5.14*10 ⁻⁹
CoTCPP/POP-Py(2)=1/1	0.154	2.33	7.84*10 ⁻⁹
CNT/CoTCPP=10/1	0.615	9.30	3.30*10 ⁻⁸

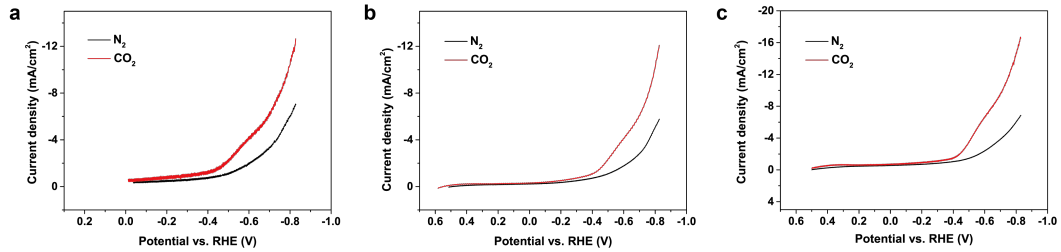


Figure S15 Linear sweep voltammetry of POP-Py(0)/CoTCPP(a), POP-Py(1)/CoTCPP (b) and POP-Py(2)/CoTCPP (c) in a 0.5 M KHCO₃ aqueous solution saturated with N₂ or CO₂.

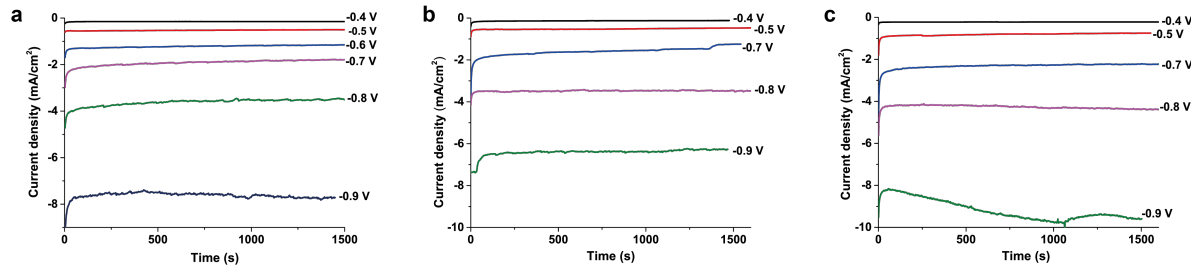


Figure S16 Representative chronoamperograms of CO₂ electroreduction catalyzed by POP-Py(0)/CoTCPP (a), POP-Py(1)/CoTCPP (b) and POP-Py(2)/CoTCPP (c) at various potentials in a 0.5 M KHCO₃ aqueous solution.

Table S3 Faradaic efficiencies and Operating durability comparison with different metal porphyrin(MPP) catalysts

Catalyst	Electrolyte	Applied potential (V vs. RHE)	I (mA/cm ²)	F.E. of CO (%)	TOF _{CO} (s ⁻¹)	Stability (hours)	Ref
POP-Py(0)/CoTCPP	0.5 M KHCO ₃	-0.6	~1.1	83	1.4	7	This work
Al ₂ (OH) ₂ TCPP-Co	0.5 M KHCO ₃	-0.7	~1	76	0.06	7	S1
CoTPP-cov	0.5 M KHCO ₃	-0.63	1.5	67	8.3	4	S2
CoTPP-noncov	0.5 M KHCO ₃	-0.63	1	52	4.4	4	S2
CoTPP/CNT	0.5 M KHCO ₃	-0.70	~3	~70	2.75	4	S3
CoP@NrGO	0.5 M NaHCO ₃	-0.70	~2.3	80	N.A.	0.5	S4
CoPP@CNT	0.5 M NaHCO ₃	-0.60	25.1	>90	1.37	12	S5
COF-367-Co	0.5 M KHCO ₃	-0.67	3.3	91	0.53	24	S6
COF-366-F-Co	0.5 M KHCO ₃	-0.67	N.A.	87	N.A.	N.A.	S7
CATpyr	0.5 M KHCO ₃	-0.59	0.24	93	0.04	3	S8

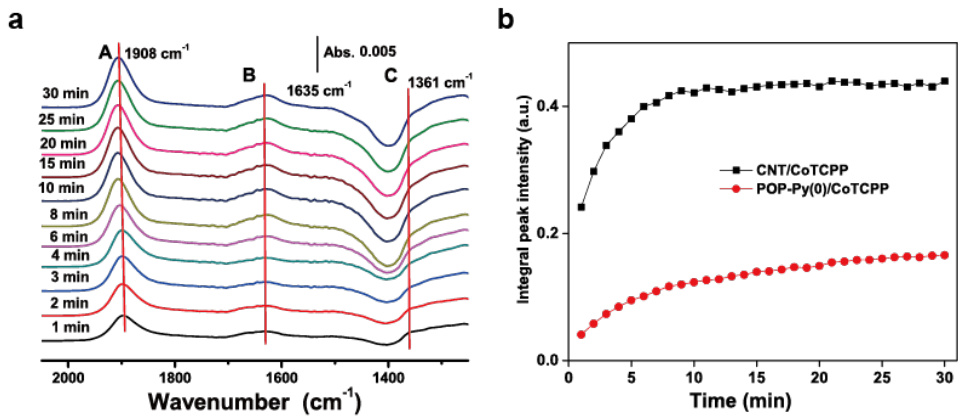


Figure S17 (a) *In-situ* ATR-SEIRAS spectra recorded with time after stepping CNT/CoTCPP to -0.6 V vs. RHE in a CO₂-saturated 0.5 M KHCO₃ aqueous solution. Reference spectrum was taken at an open circuit potential. (b) Integral intensities of peak A in the *in-situ* ATR-SEIRAS spectra of CNT/CoTCPP and POP-Py(0)/CoTCPP recorded with time at -0.6 V vs. RHE in a CO₂-saturated 0.5 M KHCO₃ aqueous solution.

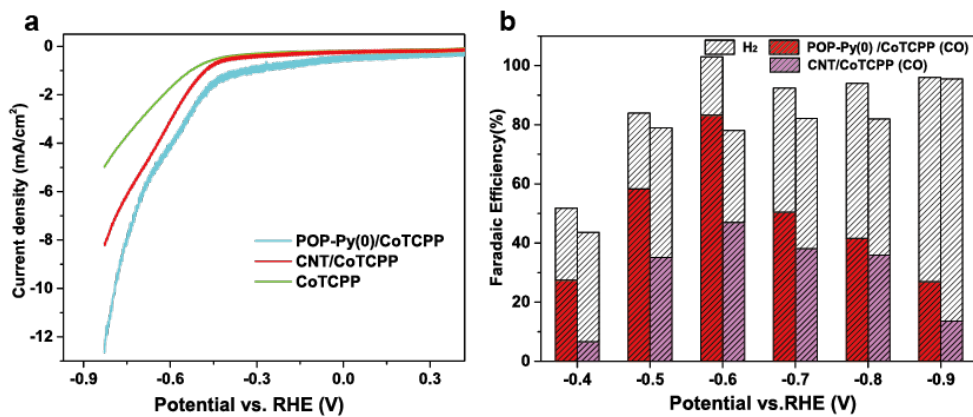


Figure S18 (a) Linear sweep voltammetry of POP-Py(0)/CoTCPP, CNT/CoTCPP and CoTCPP. (b) Faradaic efficiencies for CO and H₂ production on CNT/CoTCPP and POP-Py(0)/CoTCPP across the potential range from -0.4 to -0.9 V vs. RHE.

Table S4 Band assignments in Figure 5 and Figure S17a

Wavenumber (cm^{-1})				
POP-Py(0)/CoTCPP	POP-Py(1)/CoTCPP	POP-Py(2)/CoTCPP	CNT/CoTCPP	Assignment
1357	1354	1357	1361	$\nu(\text{C}-\text{O})$ stretching of *COOH
1643	1654	1653	1635	$\nu(\text{C}=\text{O})$ stretching of *COOH
1912-1842	1922-1859	1910-1879	1908	$\nu(\text{C}-\text{O})$ stretching of *CO(ad)

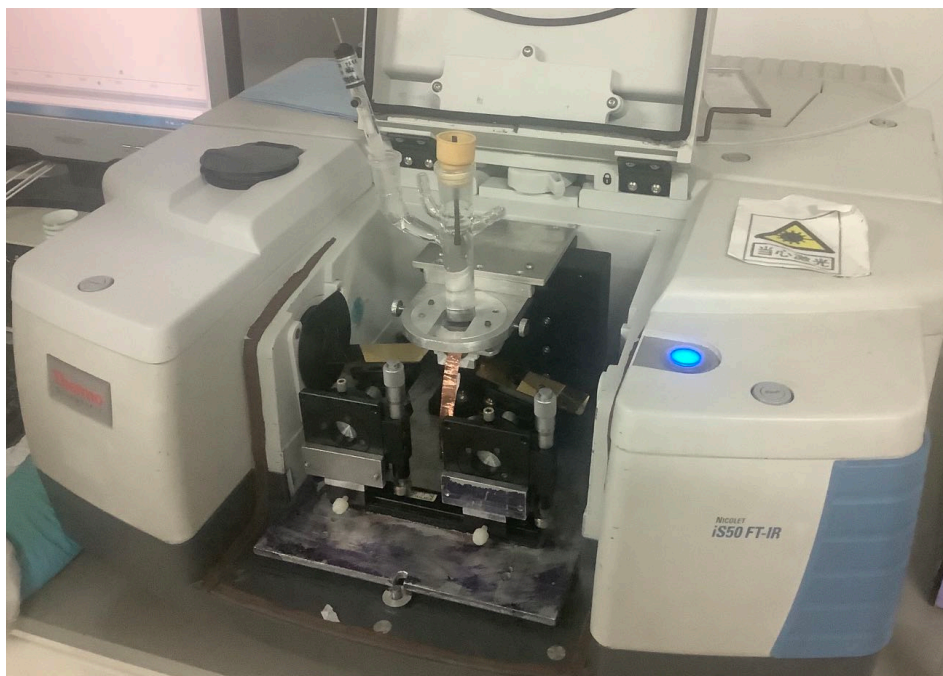


Figure S19 Cell configuration of *in-situ* SEIRAS measurements.

Reference

- S1. N. Kornienko, Y. Zhao, C. S. Kley, C. Zhu, D. Kim, S. Lin, C. J. Chang, O. M. Yaghi and P. Yang, *J. Am. Chem. Soc.*, 2015, **137**, 14129-14135.
- S2. A. N. Marianov and Y. Jiang, *Appl. Catal., B*, 2019, **244**, 881-888.
- S3 X.-M. Hu, M. H. Rønne, S. U. Pedersen, T. Skrydstrup and K. Daasbjerg, *Angew. Chem. Int. Ed.*, 2017, **56**, 6468-6472.
- S4 M. Zhu, C. Cao, J. Chen, Y. Sun, R. Ye, J. Xu, and Y.-F. Han, *ACS Appl. Energy Mater.*, 2019,

2, 2435–2440

S5 M. Zhu, J. Chen, L. Huang, R. Ye, J. Xu and Yi-Fan Han, *Angew. Chem. Int. Ed.*, 2019, **58**, 6595–6599.

S6 S. Lin, C.S. Diercks, Y.-B. Zhang, N. Kornienko, E.M. Nichols, Y. Zhao, A.R. Paris, D. Kim, P. Yang, O.M. Yaghi and C. J. Chang, *Science*, 2015, **349**, 1208–1213.

S7 C. S. Diercks, S. Lin, N. Kornienko, E. A. Kapustin, E. M. Nichols, C. Zhu, Y. Zhao, C. J. Chang and O. M. Yaghi, *J. Am. Chem. Soc.*, 2018, **140**, 1116–1122.

S8 A. Maurin and M. Robert, *J. Am. Chem. Soc.*, 2016, **138**, 2492–2495